Eur J Nucl Med Mol Imaging (2015) 42:1574–1580
DOI 10.1007/s00259-015-3089-3

ORIGINAL ARTICLE

MR-based attenuation correction for cardiac FDG PET on a hybrid PET/MRI scanner: comparison with standard CT attenuation correction

Jan Vontobel[1] · Riccardo Liga[1] · Mathias Possner[1] · Olivier F. Clerc[1] · Fran Mikulicic[1] · Patrick Veit-Haibach[1] · Edwin E. G. W. ter Voert[1] · Tobias A. Fuchs[1] · Julia Stehli[1] · Aju P. Pazhenkottil[1] · Dominik C. Benz[1] · Christoph Gräni[1] · Oliver Gaemperli[1] · Bernhard Herzog[1] · Ronny R. Buechel[1] · Philipp A. Kaufmann[1]

Received: 9 February 2015 / Accepted: 15 May 2015 / Published online: 20 June 2015

Abstract
Purpose The aim of this study was to evaluate the feasibility of attenuation correction (AC) for cardiac ^{18}F-labelled fluorodeoxyglucose (FDG) positron emission tomography (PET) using MR-based attenuation maps.
Methods We included 23 patients with no known cardiac history undergoing whole-body FDG PET/CT imaging for oncological indications on a PET/CT scanner using time-of-flight (TOF) and subsequent whole-body PET/MR imaging on an investigational hybrid PET/MRI scanner. Data sets from PET/MRI (with and without TOF) were reconstructed using MR AC and semi-quantitative segmental (20-segment model) myocardial tracer uptake (per cent of maximum) and compared to PET/CT which was reconstructed using CT AC and served as standard of reference.
Results Excellent correlations were found for regional uptake values between PET/CT and PET/MRI with TOF (n=460 segments in 23 patients; r=0.913; p<0.0001) with narrow Bland-Altman limits of agreement (−8.5 to +12.6 %). Correlation coefficients were slightly lower between PET/CT and PET/MRI without TOF (n=460 segments in 23 patients; r=0.851; p<0.0001) with broader Bland-Altman limits of agreement (−12.5 to +15.0 %). PET/MRI with and without TOF showed minimal underestimation of tracer uptake (−2.08 and −1.29 %, respectively), compared to PET/CT.
Conclusion Relative myocardial FDG uptake obtained from MR-based attenuation corrected FDG PET is highly comparable to standard CT-based attenuation corrected FDG PET, suggesting interchangeability of both AC techniques.

Keywords Cardiac imaging · Attenuation correction · PET/MRI · Hybrid imaging

Introduction

Over the past decades, hybrid positron emission tomography (PET)/CT scanners have evolved as an important non-invasive imaging tool for cardiac imaging mainly because of the added value of co-localization of functional and/or metabolic parameters acquired by PET imaging with anatomical information as depicted by coronary CT angiography [1]. PET/MRI scanners have very recently been introduced into the clinical arena as a novel type of hybrid scanner. While it is yet too early to appreciate the full spectrum of potential benefits of this technology for cardiac imaging, it may be expected that the superior assessment of left ventricular functional parameters through MRI due to excellent soft tissue characterization and improved localization of myocardial fibrosis and/or scar tissue through late contrast enhancement could provide valuable added information complementary to metabolic data assessed by PET [2, 3].

However, hybrid PET/MRI scanners lack the firmly established methods for attenuation correction (AC) provided by a dedicated CT component as in hybrid PET/CT systems.

Ronny R. Buechel and Philipp A. Kaufmann share last authorship

Jan Vontobel and Riccardo Liga contributed equally to this work.

Electronic supplementary material The online version of this article (doi:10.1007/s00259-015-3089-3) contains supplementary material, which is available to authorized users.

✉ Philipp A. Kaufmann
pak@usz.ch

[1] Department of Nuclear Medicine, University Hospital Zurich, Ramistrasse 100, 8091 Zurich, Switzerland

Calculation of accurate AC maps has been rapidly identified as a major challenge for hybrid PET/MRI systems and several approaches are currently used [4]. One approach is based on water-weighted and fat-weighted data sets derived from a Dixon MRI sequence, enabling classification of each voxel as air, lungs, fat or soft tissue [5, 6]. Bone tissue is ignored with this method as it is almost impossible to segment from such data sets. Neglecting bone tissue, however, may result in an underestimation of tissue attenuation which may be of particular concern for PET imaging of the heart which is encompassed by the rib cage and lies adjacent to the spinal column. Several studies have shown that in PET/MRI, application of MR-derived AC has led to a substantial underestimation of uptake of ^{18}F-labelled fluorodeoxyglucose (FDG) into metastases compared to PET/CT [7, 8]. A recent publication briefly assessed this issue by assessing absolute cardiac FDG uptake through regional measurement of the maximum standardized uptake value (SUV_{max}) suggesting that AC derived from MRI and CT may be interchangeable [9].

However, no comprehensive data are available on the performance of AC from MRI compared to CT for cardiac PET/MRI scanning, neither for metabolic nor for perfusion imaging. Thus, the objective of the present study was to evaluate the feasibility of AC for cardiac FDG PET using MR-based attenuation maps and testing the added value of the time-of-flight information (TOF).

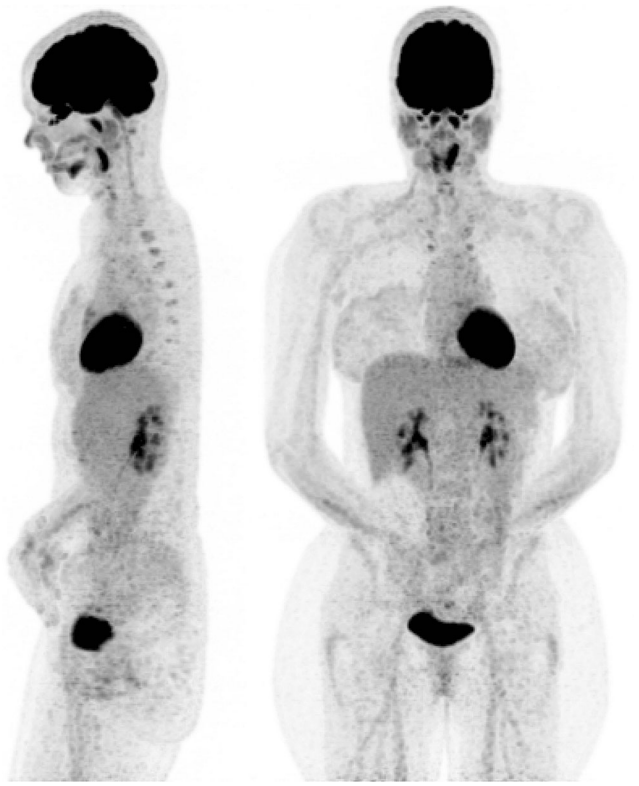

Fig. 1 Whole-body FDG PET/MRI follow-up scan of a patient with former multiple myeloma, showing spontaneous FDG accumulation in the heart

Materials and methods

Study population

A total of 43 oncological patients undergoing a clinical whole-body FDG scan on a standard PET/CT scanner were additionally scanned on an investigative simultaneous PET/MRI scanner. In a retrospective subanalysis we identified 23 patients (13 men) with spontaneous myocardial accumulation of FDG (Fig. 1). The study protocol was approved by the local Ethics Committee, and all subjects signed a written informed consent form (KEK 2013–0358, Swissmedic: 2013-MD-0035, ClinicalTrials.gov Identifier: NCT02071706).

First, a standard PET/CT scan with TOF was obtained followed by a comparative examination on a GE Signa PET/MRI hybrid whole-body scanner (GE Healthcare, Waukesha, WI, USA), which was not CE marked and not approved by the US Food and Drug Administration at the time of this study. During PET/CT scans the arms were elevated over the head, while during PET/MRI scans the arms were positioned at the side. Patients were instructed to fast for at least 4 h before FDG injection. The administered dose was 3 MBq/kg if the body weight was less than 85 kg or 3.5 MBq/kg otherwise. The mean time interval between start of the PET/CT and PET/MRI was 46±17 min (range 26–86 min).

PET/CT imaging

PET/CT images were obtained from a state-of-the-art TOF PET/CT device (Discovery D690, GE Healthcare, Waukesha, WI, USA). The Discovery 690 combines a lutetium yttrium orthosilicate (LYSO) block detector designed PET tomograph with a 64-slice CT scanner. The system further has a powerful computing platform implementing three-dimensional (3-D) PET iterative reconstruction algorithms. These algorithms can account for TOF information [10]. First, a non-contrast whole-body low-dose CT scan was acquired with a tube voltage 120–140 kV, tube current with automated dose modulation 60–440 mA/slice, collimation 64×0.625, pitch 0.984:1, rotation time 0.5 s, coverage speed 78 mm/s, transaxial field of view (FOV) 70 cm and images with a transverse pixel size of 0.625 and a slice thickness of 3.75 mm reconstructed in the axial, coronal and sagittal planes. PET data were then acquired in 3-D TOF mode with scan duration of 2 min per bed position, an overlap of bed positions of 23 % and an axial FOV of 153 mm. PET/CT data sets were reconstructed through AC of the emission data with attenuation maps obtained from the initial low-dose CT scan and were then iteratively reconstructed [matrix size 256×256, Fourier rebinning (VIP mode), VUE Point FX (3-D) with 3 iterations and 18 subsets] [11].

PET/MR imaging

After PET/CT acquisition, patients were transferred to the PET/MRI scanner which is located in an adjacent room to the PET/CT. The scanner comprises a 3-T wide-bore MRI system with an MR-compatible TOF PET detector ring installed between the body and gradient coils. The detector ring consists of 28 modules, each one containing 4×15 sub-blocks and covering roughly 64.5 × 250 mm^2. In each sub-block, an array of 3 × 2 silicon photomultipliers is paired with an array of 4 × 3 LYSO scintillator crystals, each measuring 3.95 × 5.3 × 25.0 mm^3. The PET transaxial and axial FOV are 600 and 250 mm, respectively. The best achievable resolving time of the TOF detector is less than 400 ps [12]. PET imaging time per bed position was 3 min. During continuous PET image acquisition, several MRI sequences were acquired simultaneously. First, a whole-body, dual-echo gradient recalled echo sequence (LAVA Flex) was acquired for PET AC with the body coil. From this, several reconstructions (in-phase, out-of-phase images, fat and water images) can be provided for the readers [5, 13, 14].

The following parameters were used as recently reported [11]: repetition time (TR): 4.056 ms, echo time (TE) in-phase: 2.232 ms, TE out-of-phase: 1.116 ms, flip angle (FA): 12°, FOV 500 × 375 mm (frequency × phase), acquisition matrix 256 × 128, 1 slab with 64 × 5.2 mm thick axial slices, voxel size: 1.95 × 2.93 mm and 1 average. Additionally, the basic whole-body protocol always consisted at least of a higher resolution LAVA Flex, a T_2-weighted fast recovery fast spin-echo (FRFSE) and a T_2-weighted FRFSE with fat saturation and respiratory trigger for the thorax (not simultaneously with PET). The standard patient radiofrequency (RF) coil set-up always included the 19-channel head and neck unit, the 16-channel upper and lower anterior arrays and the 14-channel central matrix array (GE Healthcare, Waukesha, WI, USA).

MR-based attenuation correction

MR AC uses a head atlas for the patient's head region and a four-class segmentation algorithm which differentiates air, lung and continuous fat/water segmentation for other body regions. In a first step the body contour is identified. In the next step the specific tissue classes (e.g. air, lung and soft tissue) are segmented with the aid of the prior knowledge of the bed positions. Next, a continuous fat-water method uses the Dixon-based MR fat and water images to allow continuous variation between fat and water classification. In the final step TOF PET data are used for truncation completion [15–17].

Table 1 Patient baseline characteristics and reason for referral

Patient	Diagnosis	Age (years)	BMI (kg/m^2)
1	Metastasizing adenocarcinoma of the lung	50	21.3
2	Hodgkin's lymphoma	30	22.8
3	Adenocarcinoma of the lung	58	22.1
4	Sigma carcinoma	55	28.7
5	Metastasizing carcinoma of the breast	53	26.0
6	Squamous cell carcinoma of the parotid gland	58	25.1
7	Carcinoma of the tongue	51	23.3
8	Multiple myeloma	57	21.7
9	Non-Hodgkin's lymphoma	41	25.4
10	Squamous cell carcinoma of the tonsil	57	19.8
11	Rectum carcinoma	51	19.0
12	Mantle cell non-Hodgkin's lymphoma	54	22.6
13	Invasive ductal carcinoma of the breast	41	18.3
14	Adenocarcinoma of the lung	52	28.3
15	B-cell lymphoma	73	26.2
16	Metastasizing melanoma	45	30.8
17	Squamous cell carcinoma of the cheek	62	26.8
18	Nodular melanoma of the thigh	71	29.4
19	Metastasizing melanoma	63	31.0
20	Squamous cell carcinoma of the lung	64	21.6
21	Mucoepidermoid carcinoma of the sublingual gland	48	28.6
22	Carcinoma of the prostate	70	31.6
23	Anal carcinoma	70	25.3

BMI body mass index

To assess the impact of TOF on MR attenuation maps, all PET images from PET/MRI were reconstructed without TOF and with TOF for each data set. The first applied method, VUE Point HD (VPHD), is based on a fully 3-D ordered subsets expectation maximization (3-D OSEM) iterative reconstruction algorithm, which incorporates all corrections (scatter, random, dead time, attenuation and normalization) but ignores the TOF information. The second applied method, VUE Point FX (VPFX), is similar to VPHD but takes the TOF information into account.

PET analysis

PET data were analysed using a commercially available software package (Myovation, GE Healthcare, Waukesha, WI, USA) on a dedicated imaging workstation (Xeleris 3, GE Healthcare, Waukesha, WI, USA). Polar maps were normalized to 100 % peak activity and the segmental relative radiotracer uptake was computed using a 20-segment model for the left ventricle [18]. The effect of CT AC may vary substantially among different myocardial regions owing to anatomical non-uniformity or misalignment, as demonstrated by Ficaro et al. [19] and Lautamäki et al. [20]. In order to assess such variations among myocardial regions we also assigned the 20 segments of the left ventricular myocardium to five regions of the left ventricle for regional comparison: apex (segments 19 and 20), anterior (segments 1, 2, 7, 8, 13 and 14), septal (segments 3, 9 and 15), lateral (segments 5, 6, 11, 12, 17 and 18) and inferior (segments 4, 10 and 16) [21]. Analysis was performed with CT AC and repeated with MR AC (with and without TOF).

Statistical analysis

Values are expressed as mean±standard deviation. Pearson correlation and Bland-Altman analysis (BA) [22] were used for evaluation of the continuous values. All statistical analyses were performed using a commercially available software package (IBM SPSS Statistics, Version 22). A p value<0.05 was considered statistically significant.

Results

Baseline characteristics and reason for referral for each individual study patient are given in Table 1. The mean age was 55±10 years (range 30–73 years), and mean body mass index was 25±3.8 kg/m^2. All 23 patient data sets were successfully

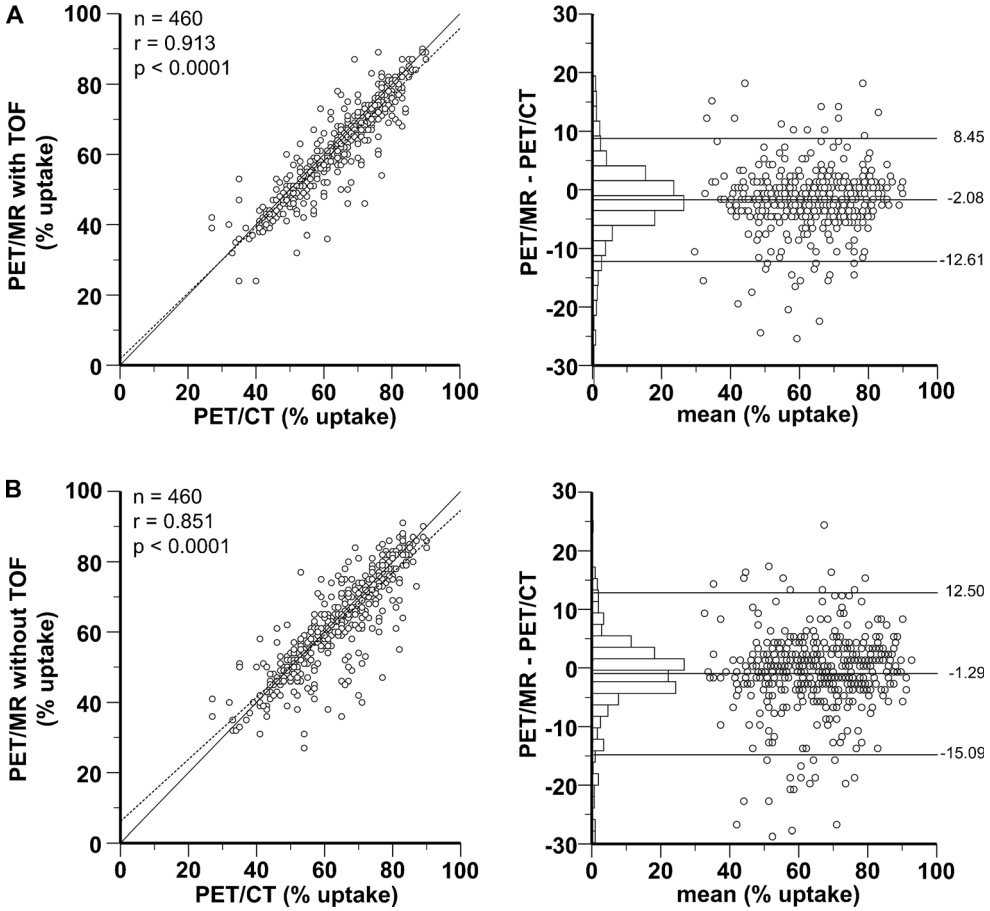

Fig. 2 Linear regression analysis and Bland-Altman plots for comparison of segmental per cent FDG uptake from PET/MRI versus PET/CT using PET/MRI with TOF (**a**) or without TOF (**b**). The histogram on the y-axis in the Bland-Altman plots depicts the frequency of differences in segmental uptake

Table 2 Correlation coefficients and BA agreement between CT AC and MR AC with TOF and between CT AC and MR AC without TOF for various myocardial regions ($p<0.0001$ for all correlations)

		Apical CT AC	Anterior CT AC	Septal CT AC	Lateral CT AC	Inferior CT AC
MR AC with TOF	CC	0.918	0.897	0.946	0.891	0.922
	BA	+7.14 to–13.92	+10.38 to–13.88	+7.85 to–8.81	+7.77 to–3.36	+6.02 to–0.46
	Mean[a]	–3.38	–1.65	–0.48	–2.78	–2.22
MR AC without TOF	CC	0.928	0.812	0.903	0.821	0.861
	BA	+8.96 to–11.41	+15.74 to–16.84	+11.07 to–12.03	+10.38 to–16.80	+11.69 to–10.46
	Mean[a]	–1.28	–0.55	–0.48	–3.21	+0.26

AC attenuation correction, *CC* correlation coefficients, *TOF* time of flight, *BA* Bland-Altman limits of agreement (%)

[a] Mean difference between PET/MRI and PET/CT (i.e. PET/MRI − PET/CT)

analysed from both scanners, resulting in 460 segments and 5 regions. Of note, no patient had a history of coronary artery disease.

Compared to PET/CT AC, PET/MRI AC with TOF and PET/MRI without TOF both showed minimal, but statistically significant, underestimation of tracer uptake of −2.08 and −1.29 %, respectively (both $p<0.0001$) (Fig. 2a, b). Comparison of segmental FDG uptake between PET/CT and PET/MRI (both with TOF) revealed an excellent correlation ($n=460$; $r=0.913$; $p<0.0001$) with narrow limits of agreement (−12.61 to +8.45 %) (Fig. 2a). After switching off the TOF information in PET/MRI the correlation was slightly weaker ($r=0.851$; $p<0.0001$) with slightly broader limits of agreement (−15.09 to +12.50 %) (Fig. 2b).

Similarly, the correlations between regional radiotracer uptake values obtained from PET/MRI AC with TOF and PET/CT AC were highly significant, with correlation coefficients ranging from 0.891 to 0.946 (Table 2) and narrow limits of agreement (apex, +7.14 to −13.92 %, mean −3.38; anterior, +10.38 to −13.88 %, mean −1.65; septal, +7.85 to −8.81 %, mean −0.48; lateral, +7.77 to −13.36 %, mean −2.78; inferior, +6.02 to −10.46 %, mean −2.22). Similarly, excellent correlations between regional FDG uptake values obtained from PET/MRI without TOF and PET/CT AC were found with coefficients ranging from 0.812 to 0.928 (Table 2) and narrow limits of agreement (apex, +8.96 to −11.41 %, mean −1.28; anterior, +15.74 to −16.84 %, mean −0.55; septal, +11.07 to −12.03 %, mean −0.48; lateral, +10.38 to −16.80 %, mean −3.21; inferior, +11.69 to −10.46 %, mean +0.26). These findings are consistent with a visual reading of the polar maps which showed comparable perfusion distribution in between MR AC without TOF, MR AC with TOF and CT AC with TOF (Fig. 3). For a more detailed analysis a segment-wise evaluation is summarized in the supplementary data.

Discussion

Hybrid PET/MRI is emerging as a novel diagnostic modality for cardiac imaging with the promise of playing an exciting role in multiple cardiovascular applications [2, 23]. Contrary to PET/CT, however, hybrid PET/MRI does not directly provide the data needed for AC as the signal intensity in the MR image is not directly related to photon attenuation. Current techniques for MR-based AC rely on attenuation maps derived from image segmentation where the MR image is segmented into different tissues with similar tissue characteristics for attenuation coefficients to be assigned based on known attenuation coefficients [4, 5]. The present study aims at evaluating the feasibility of such a segmentation-based approach for cardiac FDG PET by comparing relative segmental

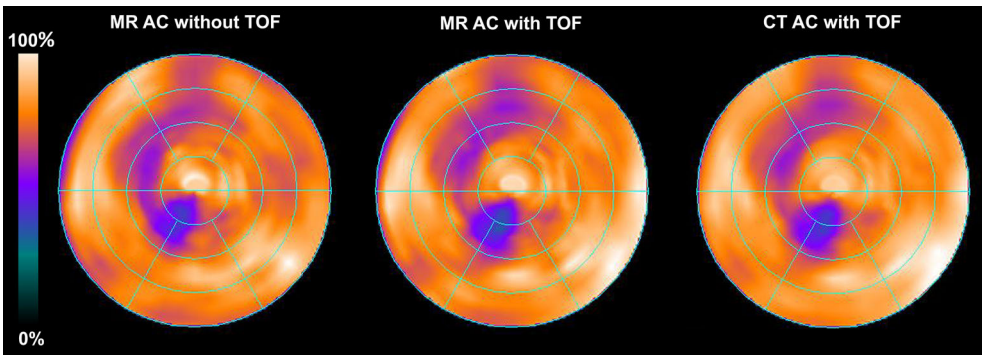

Fig. 3 Polar maps representing segmental per cent myocardial FDG uptake in a single patient, reconstructed using MR AC without TOF, MR AC with TOF or CT AC with TOF

myocardial tracer uptake obtained from a novel hybrid PET/MRI device versus standard PET/CT.

Our results demonstrate an excellent comparability among the two AC techniques with relative segmental tracer uptake from PET/MRI highly correlating with results from PET/CT and with minimal underestimation by PET/MRI and narrow limits of agreement within a clinically acceptable range [24].

Furthermore, we evaluated the potential added value from integrating PET TOF information into the reconstruction of PET/MR images. Conventional non-TOF PET detector systems assume that photons arriving at two opposite detectors, within a predefined timing window of a few nanoseconds, originated from an annihilation event that could have occurred anywhere along the line of response between the two detectors with equal probability. A TOF PET detector system can measure the time difference between the two photons arriving at opposite detectors with a certain resolution [25, 26]. As a result, TOF allows better localization of annihilation, enables better lesion detectability and improves the signal to noise ratio [27]. This could potentially contribute to overcoming some of the limitations of AC in PET/MRI, such as segmentation error and artefacts due to bone or metal implants, which may lead to inconsistencies in MR AC maps, thereby affecting diagnostic accuracy of PET [28]. In the present study, the addition of TOF information for AC in PET/MRI substantially improved the correlation with AC of PET/CT, notably with narrower BA limits of agreement compared to PET/MRI AC without TOF. Similarly, comparison of regional uptake values revealed a slightly superior agreement of PET/MRI AC with TOF particularly in the anterior, inferior and lateral segments. Of note, for MR AC without TOF BA analysis revealed a slight overestimation of tracer uptake in the inferior wall. By contrast MR AC with TOF led to a small underestimation of tracer uptake which was consistent across all regions. Thus, if available in modern PET systems, the additional information from TOF should be integrated into the process of AC.

In summary, albeit by using Dixon sequences for MR AC no specific correction for photon attenuation from bone tissue could be applied, our findings suggest interchangeability of MR AC with conventional CT AC for the non-quantitative assessment of cardiac FDG uptake as it is routinely performed for evaluation of myocardial viability. Whether addition of attenuation information for bone tissue, for example through application of ultrashort echo time MRI sequences, would have improved our results remains to be evaluated [29]. These findings are in line with a recent publication evaluating absolute cardiac FDG uptake from MR-based AC as assessed by SUV_{max} values [8]. Our findings may not necessarily apply to other cardiac PET applications such as perfusion scanning including qualitative and quantitative perfusion assessment and functional parameters from gated acquisition.

Although our findings have to be confirmed in future studies in larger patient populations and in a real-world clinical setting, they have important preliminary implications for future cardiac PET/MRI protocols, because validation of MR AC is imperative for rendering the CT scans unnecessary in the future, thereby setting the grounds for hybrid cardiac PET/MRI to play out its full potential in the future.

We acknowledge several limitations of our study. First, we analysed FDG data sets that were acquired in an oncological setting with spontaneous accumulation of FDG in the heart rather than from specific cardiac viability evaluation. Second, PET/MRI AC and PET/CT AC were not acquired simultaneously and the time interval between the two scans may have potentially affected the comparability of tracer uptake due to inhomogeneous tracer washout in different cardiac segments. Furthermore, the scanners used in the present study differ in terms of system design, and image data sets obtained are specifically dependent on the applied reconstruction algorithms and acquisition durations. However, it appears that this has not affected the agreement between the two methods, which strengthens the results of our study. Finally, our results may at least in part be scanner specific and therefore not necessarily applicable to other scanners from other vendors.

Conclusion

Relative myocardial FDG uptake obtained from MR-based attenuation-corrected FDG PET is highly comparable to standard CT-based attenuation-corrected FDG PET, suggesting interchangeability of both AC techniques.

Compliance with ethical standards All procedures performed in this study were in accordance with the ethical standards of the national research committee and with the 1964 Declaration of Helsinki and its later amendments or comparable ethical standards. Informed consent was obtained from all individual participants.

Conflicts of interest None.

Financial support The University Hospital Zurich holds a research contract with GE Healthcare.

References

1. Bengel FM, Higuchi T, Javadi MS, Lautamäki R. Cardiac positron emission tomography. J Am Coll Cardiol 2009;54:1–15.
2. Rischpler C, Nekolla SG, Dregely I, Schwaiger M. Hybrid PET/MR imaging of the heart: potential, initial experiences, and future prospects. J Nucl Med 2013;54:402–15.
3. von Schulthess GK, Kuhn FP, Kaufmann P, Veit-Haibach P. Clinical positron emission tomography/magnetic resonance imaging applications. Semin Nucl Med 2013;43:3–10.
4. Hofmann M, Pichler B, Schölkopf B, Beyer T. Towards quantitative PET/MRI: a review of MR-based attenuation correction techniques. Eur J Nucl Med Mol Imaging 2009;36 Suppl 1:S93–104.
5. Coombs BD, Szumowski J, Coshow W. Two-point Dixon technique for water-fat signal decomposition with B0 inhomogeneity correction. Magn Reson Med 1997;38:884–9.

6. Wollenweber SD AS, Lonn AHR, Shanbhag DD, Thiruvenkadam S, Kaushik S, Mullick R, et al. Comparison of 4-class and continuous fat/water methods for whole-body, MR-based PET attenuation correction. Nuclear Science Symposium and Medical Imaging Conference (NSS/MIC). 2012:3019–3025.
7. Samarin A, Burger C, Wollenweber SD, Crook DW, Schmid DT, von Schulthess GK, et al. PET/MR imaging of bone lesions–implications for PET quantification from imperfect attenuation correction. Eur J Nucl Med Mol Imaging 2012;39:1154–60.
8. Izquierdo-Garcia D, Sawiak SJ, Knesaurek K, Narula J, Fuster V, Machac J, et al. Comparison of MR-based attenuation correction and CT-based attenuation correction of whole-body PET/MR imaging. Eur J Nucl Med Mol Imaging 2014;41:1574–84.
9. Nensa F, Poeppel TD, Beiderwellen K, Schelhorn J, Mahabadi AA, Erbel R, et al. Hybrid PET/MR imaging of the heart: feasibility and initial results. Radiology 2013;268:366–73.
10. Bettinardi V, Presotto L, Rapisarda E, Picchio M, Gianolli L, Gilardi MC. Physical performance of the new hybrid PET/CT Discovery-690. Med Phys 2011;38:5394–411.
11. Queiroz MA, Hüllner M, Kuhn F, Huber G, Meerwein C, Kollias S, et al. PET/MRI and PET/CT in follow-up of head and neck cancer patients. Eur J Nucl Med Mol Imaging 2014;41:1066–75.
12. Davison H, Ter Voert EE, de Galiza Barbosa F, Veit-Haibach P, Delso G. Incorporation of time-of-flight information reduces metal artifacts in simultaneous positron emission tomography/magnetic resonance imaging: a simulation study. Invest Radiol 2015.
13. Dixon WT. Simple proton spectroscopic imaging. Radiology 1984;153:189–94.
14. Bley TA, Wieben O, François CJ, Brittain JH, Reeder SB. Fat and water magnetic resonance imaging. J Magn Reson Imaging 2010;31:4–18.
15. Martinez-Möller A, Souvatzoglou M, Delso G, Bundschuh RA, Chefd'hotel C, Ziegler SI, et al. Tissue classification as a potential approach for attenuation correction in whole-body PET/MRI: evaluation with PET/CT data. J Nucl Med 2009;50:520–6.
16. Wollenweber SD, Ambwani S, Lonn AHR, et al. Comparison of 4-class and continuous fat/water methods for whole-body, MR-based PET attenuation correction. Paper presented at: Nuclear Science Symposium and Medical Imaging Conference (NSS/MIC), 2012 IEEE; 27 Oct 2012–3 Nov 2012.
17. Wollenweber SDAS, Lonn AHR, et al. Comparison of 4-class and continuous fat/water methods for whole-body, MR-based PET attenuation correction. IEEE Trans Nucl Sci 2012;60(5):3391–8.
18. Cerqueira MD, Weissman NJ, Dilsizian V, Jacobs AK, Kaul S, Laskey WK, et al. Standardized myocardial segmentation and nomenclature for tomographic imaging of the heart. A statement for healthcare professionals from the Cardiac Imaging Committee of the Council on Clinical Cardiology of the American Heart Association. Int J Cardiovasc Imaging 2002;18:539–42.
19. Ficaro EP, Fessler JA, Ackermann RJ, Rogers WL, Corbett JR, Schwaiger M. Simultaneous transmission-emission thallium-201 cardiac SPECT: effect of attenuation correction on myocardial tracer distribution. J Nucl Med 1995;36:921–31.
20. Lautamäki R, Brown TL, Merrill J, Bengel FM. CT-based attenuation correction in (82)Rb-myocardial perfusion PET-CT: incidence of misalignment and effect on regional tracer distribution. Eur J Nucl Med Mol Imaging 2008;35:305–10.
21. Schepis T, Gaemperli O, Koepfli P, Rüegg C, Burger C, Leschka S, et al. Use of coronary calcium score scans from stand-alone multislice computed tomography for attenuation correction of myocardial perfusion SPECT. Eur J Nucl Med Mol Imaging 2007;34:11–9.
22. Bland JM, Altman DG. Statistical methods for assessing agreement between two methods of clinical measurement. Lancet 1986;1:307–10.
23. Adenaw N, Salerno M. PET/MRI: current state of the art and future potential for cardiovascular applications. J Nucl Cardiol 2013;20:976–89.
24. Bailey DL, Barthel H, Beuthin-Baumann B, Beyer T, Bisdas S, Boellaard R, et al. Combined PET/MR: where are we now? Summary report of the second international workshop on PET/MR imaging April 8–12, 2013, Tubingen, Germany. Mol Imaging Biol 2014;16:295–310.
25. Budinger TF. Time-of-flight positron emission tomography: status relative to conventional PET. J Nucl Med 1983;24:73–8.
26. Moses W. Time of flight in PET revisited. IEEE Trans Nucl Sci 2003;50:1325–30.
27. Surti S, Karp JS. Experimental evaluation of a simple lesion detection task with time-of-flight PET. Phys Med Biol 2009;54:373–84.
28. Surti S. Update on time-of-flight PET imaging. J Nucl Med 2015;56:98–105.
29. Keereman V, Fierens Y, Broux T, De Deene Y, Lonneux M, Vandenberghe S. MRI-based attenuation correction for PET/MRI using ultrashort echo time sequences. J Nucl Med 2010;51:812–8.